

Geophysical Research Letters®



RESEARCH LETTER

10.1029/2024GL108565

Urbanization Further Intensifies Short-Duration Rainfall Extremes in a Warmer Climate

Key Points:

- Non-stationarities of sub-daily rainfall extremes over a coastal megalopolis exhibit marked land cover and duration dependencies
- Urban areas show more prominent intensification of events over short durations and short return periods compared with rural areas
- Rural areas show smaller nonstationary variabilities across durations and return periods and a lower peak scaling rate than urban areas

Supporting Information:

Supporting Information may be found in the online version of this article.

Correspondence to:

M. Guan,
mfguan@hku.hk

Citation:

Yan, H., Gao, Y., Wilby, R., Yu, D., Wright, N., Yin, J., et al. (2024). Urbanization further intensifies short-duration rainfall extremes in a warmer climate. *Geophysical Research Letters*, 51, e2024GL108565. <https://doi.org/10.1029/2024GL108565>

Received 29 JAN 2024

Accepted 26 FEB 2024

Author Contributions:

Conceptualization: Haochen Yan, Mingfu Guan

Data curation: Haochen Yan, Xunlai Chen, Mingfu Guan

Formal analysis: Haochen Yan

Funding acquisition: Mingfu Guan

Investigation: Haochen Yan, Yao Gao

Methodology: Haochen Yan

Project administration: Mingfu Guan






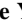



Resources: Xunlai Chen

Supervision: Mingfu Guan

Visualization: Haochen Yan

Writing – original draft: Haochen Yan, Mingfu Guan

Writing – review & editing: Yao Gao, Robert Wilby, Dapeng Yu, Nigel Wright, Jie Yin, Ji Chen

Haochen Yan¹ , Yao Gao^{1,2} , Robert Wilby³ , Dapeng Yu³ , Nigel Wright⁴ , Jie Yin⁵ , Xunlai Chen⁶ , Ji Chen¹ , and Mingfu Guan¹ 

¹Department of Civil Engineering, the University of Hong Kong, Hong Kong SAR, China, ²Finnish Meteorological Institute, Helsinki, Finland, ³Geography and Environment, Loughborough University, Loughborough, UK, ⁴School of Engineering, University of Birmingham, Birmingham, UK, ⁵Key Laboratory of Geographic Information Science (Ministry of Education), East China Normal University, Shanghai, China, ⁶Shenzhen Meteorological Bureau, Shenzhen, China

Abstract Intensification of short-duration rainfall extremes contributes to increased urban flood risk. Yet, it remains unclear how upper-tail rainfall statistics could change with regional warming. Here, we characterize the non-stationarity of rainfall extremes over durations of 1–24 hr for the rapidly developing coastal megalopolis of the Greater Bay Area, China. Using high-resolution, multi-source, merged and gridded data we observe greater increases in rainfall intensities over the north-central part of the region compared with the southern coastal region. Our results show, for the first time, that urbanization nonlinearly increases rainfall intensities at different durations and return periods. Over short durations (≤ 3 -hr) and short return periods (2-yr), urban areas have the greatest scaling rates ($\geq 19.9\%/^{\circ}\text{C}$). However, over longer durations (≥ 9 -hr) rural areas have greater scaling rates, with a lower degree of dependency on both durations and return periods.

Plain Language Summary Short-duration (sub-daily) rainfall extremes are major drivers of flash floods and hence significant disruptions to society. Previous modeling and statistical studies show that urbanization intensifies short-duration rainfall extremes. However, there has been less attention to regional variations in rates of rainfall intensification under a warming climate, particularly for extreme events with return periods that are comparable to or longer than the years of record. In this study, we investigate changes in rainfall extremes over the Greater Bay Area, China using long records of high-resolution data merged from gauge networks, satellite observations, and reanalysis products. This enables us to evaluate changes in low-frequency rainfall extremes (2- to 100-yr return periods) over different land surfaces, under a warming climate. We find that increases in rainfall extremes significantly depend on the duration and return period of events, with the largest scaling occurring for short-duration “nuisance” rainfall intensities over urban areas.

1. Introduction

Heavy precipitation has increased in intensity and frequency for most land areas since the 1950s—trends that have been attributed to human-induced global warming (IPCC, 2021). Although such changes at daily or longer durations are detected globally (IPCC, 2021; Papalexou & Montanari, 2019; Westra et al., 2013), sub-daily rainfall extremes, which can cause severe socioeconomic impacts through flash flooding (Ayat et al., 2022; Fischer & Knutti, 2016; Fowler et al., 2021), generally exhibit much greater variability across continents, regions, and sites (Agilan & Umamahesh, 2015; Barbero et al., 2017; Chen et al., 2021; Fowler et al., 2021; Hosseinzadehtalaei et al., 2020). In urban areas, where more than half of the global population is concentrated (Grimm et al., 2008), rainfall patterns are modified by the (a) heat island, (b) higher surface roughness, (c) higher aerosol concentrations and (d) land use, which collectively enhance extreme and total rainfall, both locally and downwind (Han et al., 2014; Liu & Niyogi, 2019; Shepherd, 2013). Hence, continuous and rapid urbanization are exposing larger populations to flood risk, especially in the economic growth hubs of the Asia-Pacific region.

Extreme value theory (EVT) is typically used to evaluate the statistical properties of rainfall extremes, so that events beyond the range of available data can be estimated (Khaliq et al., 2006). Associated methodologies such as intensity-duration-frequency (IDF) curves are routinely applied to infrastructure design and water management (Hosseinzadehtalaei et al., 2020). However, these conventional techniques rest on the assumption of stationarity which is problematic in the context of climate change, as the probability distribution of the extreme variable studied is time-invariant (Khaliq et al., 2006; Milly et al., 2008). Hence, as seen worldwide (Fauer & Rust, 2022; Fu et al., 2021; Slater et al., 2021), it makes sense to consider the non-stationarity of rainfall extremes using EVT.

© 2024. The Authors.

This is an open access article under the terms of the [Creative Commons Attribution License](https://creativecommons.org/licenses/by/4.0/), which permits use, distribution and reproduction in any medium, provided the original work is properly cited.

Unfortunately, rain gauge networks—which are often used for extreme value analysis—have uneven and sparse coverage and may under- or mis-sample localized convective events which largely contribute to short-duration extremes (Kidd et al., 2017; Lengfeld et al., 2020). On the other hand, satellite-derived and/or model-based precipitation products offer finer spatiotemporal resolutions and better spatial coverage (Sun et al., 2018). Nevertheless, they are inadequate for regional extreme value analysis due to significant uncertainties in their accuracy (Alexander et al., 2019; Ali et al., 2021; Zhang et al., 2022). In this regard, blending multiple sources for long-term rainfall statistics characterization is recommended (e.g., McLeod et al., 2017; McLeod & Shepherd, 2022), while those on the non-stationarity of rainfall extremes at an hourly scale are scanty.

Increasing intensities of sub-daily rainfall in urbanized areas has been detected by nonstationary EVT using a few stations (Agilan & Umamahesh, 2015; Ganguli & Coulibaly, 2017; Yilmaz et al., 2014) (Figure S1, Table S1 in Supporting Information S1). However, duration- and land-use dependent variations in sub-daily rainfall extremes—such as between rural and urban areas—remain unclear. Statistical relationships between non-stationarity and underlying climate drivers, implied by time and physical covariates formulated in frequency models, further complicate planning by city authorities who are contending with urban growth and rising temperatures (Chen et al., 2013; Fauer & Rust, 2022; Westra & Sisson, 2011). Many studies have applied Clausius–Clapeyron (C–C) scaling to describe how the moisture-holding capacity of the atmosphere and thus rainfall intensity responds to global/regional warming (Bao et al., 2017; Lenderink & van Meijgaard, 2008; Visser et al., 2021; Westra et al., 2014). Most relate extreme quantiles to incremental temperature bins, usually at daily timescales (Fowler et al., 2021). However, scaling of “upper tail”, short-duration rainfall intensities (at return periods well beyond the length of typical observational records) is hitherto unexplored.

Here, we analyze non-stationarity in hourly to daily rainfall extremes (at return periods ≥ 2 yr) linked to surface temperatures over the Greater Bay Area (GBA). The GBA is an agglomeration of 11 metropolitan areas in south China covering Guangdong, Hong Kong and Macau. This region has experienced a surge in urban development and population growth since the 1990s, becoming one of the most important economic hubs in Asia (Qiang et al., 2020; Sun et al., 2021). Moreover, the GBA is amongst the most vulnerable urban areas globally, given its high exposure to floods, dense population, and developing economy (Schelske et al., 2013). Having differentiated areas with high and low degrees of urbanization, we investigate non-stationarity in rainfall extremes over the region at hourly to daily scales, alongside potential climate drivers. Robust scaling relationships are then derived for duration-, return-period, and land cover dependent rainfall extremes.

2. Materials and Methods

2.1. Meteorological Data and Multisource Merging

This study applied nonstationary frequency analysis to high spatial-resolution hourly rainfall data. The gridded rainfall data used included the Multi-Source Weighted-Ensemble Precipitation (MSWEP V2.8) product (Beck et al., 2019), Integrated Multi-satellite Retrievals for the Global Precipitation Measurement mission (IMERG) Final Run Version 07 (Huffman et al., 2023), and the ERA5-Land reanalysis data of the European Center for Medium-Range Weather Forecast (ECMWF) (Hersbach et al., 2020). In addition, rain gauge data from 50 weather stations managed by the National Meteorological Information Center of the China Meteorological Administration and The Hong Kong Observatory were also analyzed. Other meteorological data, covering the period 1960–2020, included global (land air + sea water) mean surface temperature, Multivariate ENSO Index (MEI), mean surface air temperature (T2m), mean dew point temperature (DT2m), and mean equivalent potential temperature (EPT). The T2m and DT2m data were obtained from the ERA5-Land dataset, whereas EPT was calculated following the methods in Song et al. (2022).

2.2. Multisource Merging and Correction of the Gridded Rainfall Data

Quality assessment of several gridded rainfall products for the GBA showed poor agreement with hourly gauge observations (Figure S2 in Supporting Information S1). Although preliminary calibration was performed for the multi-source merged products such as MSWEP, only a limited number of gauges with daily data were incorporated (Beck et al., 2019; Hersbach et al., 2020). Thus, we further employed a Random Forest-based Merging Procedure (RF-MEP) (Baez-Villanueva et al., 2020) to the original datasets described in Section 2.1 to improve their spatiotemporal accuracy at hourly, 0.1° resolutions. The RF-MEP dataset significantly improved the original

data in terms of the Nash–Sutcliffe efficiency (NSE) coefficient whilst also preserving spatial details beyond that of the gauge network (Text S1, Figure S2 in Supporting Information S1).

2.3. Nonstationary Frequency Analysis of Rainfall Extremes

Annual maximum rainfall intensities were extracted for each grid/station under various durations for frequency analysis. “Rainfall extremes” refer to rainfall intensities with ≥ 2 -yr return periods. This criterion is roughly equivalent to the 98.75th and 99.7th percentiles in terms of event-based and direct sampling of hourly time series, respectively. The Generalized Extreme Value (GEV) distribution was applied with flexible location and scale parameters. Climate variables were then used as physical covariates to represent any non-stationarity (Coles et al., 2003; Nerantzaki & Papalexiou, 2022). Details of the model structure, model selection, and parameter estimation are given in Text S2 in Supporting Information S1. Mann–Kendall (M–K) trend analysis with Sen’s slope estimator (Gocic & Trajkovic, 2013; Khaliq et al., 2009) was performed for each location/grid for different return periods.

2.4. Classification of Urban and Rural Areas

The non-stationarity of rainfall extremes in rural and land areas were compared by differentiating the grids based on the land cover conditions. The 0.1° grids with a built-up land fraction of $\geq 5\%$ in 1980 or went through $\geq 5\%$ increase of the built-up land fraction during 1980–2018 were classified as urban group, yielding about 56% rural grids and 44% urban grids (more details are given in Test S3 in Supporting Information S1). In addition, potential climate drivers of the detected non-stationarity, such as mesoscale convective systems, tropical cyclones, and monsoonal activities, were also evaluated in association with land covers (Text S4 in Supporting Information S1).

2.5. Surface Temperature Scaling of Nonstationary Return Periods

To evaluate how nonstationary (NS) rainfall extremes respond to regional warming, we calculated scaling of rainfall intensities at different return periods (RP) with respect to annual mean surface temperature, or the NS-RP scaling for simplicity. Such scaling attempts to relate rainfall intensities corresponding to a certain exceedance probability under a changing climate to more readily accessible and certain climate variables (e.g., annual mean surface air temperature, AMSAT). Similar to the scaling in the time domain (Bao et al., 2017; Lenderink & van Meijgaard, 2008; Visser et al., 2021), the NS-RP scaling assumes that changes in the AMSAT ΔT are associated with $\alpha\%$ changes in rainfall extreme intensities, such that:

$$P_{2,T,RL} = (1 + 0.01\alpha)^{\Delta T} P_{1,T,RL} \quad (3)$$

where $P_{1,T,RL}$ and $P_{2,T,RL}$ are the average rain intensity for a given RL of specified event duration (T) in periods 1 and 2, respectively, whilst ΔT is the difference in the AMSAT of the corresponding two periods. Re-arrangement of the above equation yields:

$$\alpha = \left[\frac{\ln(P_{2,T,RL}/P_{1,T,RL})}{\Delta T} - 1 \right] \times 100 \quad (4)$$

We applied bootstrapping to estimate α at each grid by randomly sampling two equal-length subperiods with replacement, with repetition of 500 times. Then, the median $\alpha\%$ from all the repetitions was recorded as the representative scaling rate of the grid.

3. Results

3.1. Non-Stationarity With Event Duration-Dependency

Overall, increasing trends are detected in both the annual maximum (AMAX) and nonstationary (NS) frequency of 10-yr hourly rainfall intensities at gauge stations in the GBA (Figures 1a and 1b). For the hourly duration, more than 60% of stations show positive trends, primarily in the central part of the region. For the daily duration, less than 50% of stations have positive NS trends (Figures 1c and 1d). Only a few stations (12% for hourly and 10% for daily durations) have statistically significant trends ($\alpha \leq 0.05$) for AMAX, suggesting that the AMAX is less able to detect non-stationarity than NS for which 12% and 36% of stations have significant trends in terms of hourly

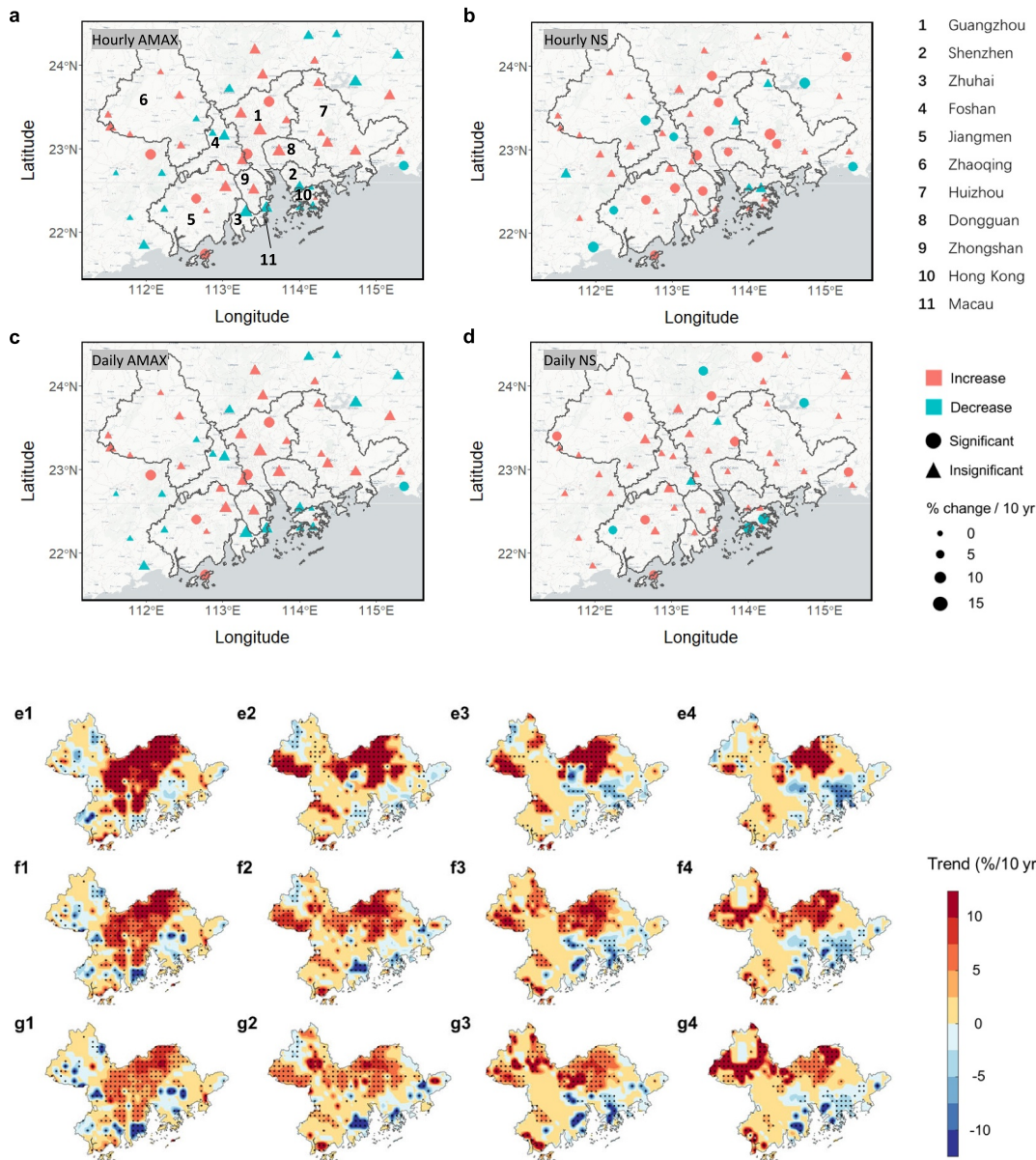


Figure 1. Nonstationary short-duration rainfall extremes detected by gauges and multisource-merged gridded data. Trends in annual maximum (AMAX) rainfall intensity for (a) 1-hr and (c) 24-hr durations were normalized by the local mean annual maximum intensities, and the trends in nonstationary (NS) 10-yr return level for (b) 1-hr and (d) 24-hr durations were normalized by stationary model results. Positive and negative trends are denoted by red and green colors of symbols, with triangles and circles marking the significance level ($\alpha \leq 0.05$ for significant); symbol sizes represent trend magnitudes. (e1)–(g4), spatially uneven nonstationary rainfall extremes given by the trend normalized by the stationary model results at 2- (e), 10- (f), and 100-yr (g) return periods for 1-, 6-, 12- and 24 hr durations (numbered 1–4). Dots mark grids with significant trends ($\alpha \leq 0.05$).

AMAX and NS, respectively. Guangzhou (the north-central part of the GBA) has most rapid changes in rainfall extremes at both hourly and daily scales. Here, trends for hourly and daily intensities are around +15%/10 yr for AMAX, and around +7%/10 yr for NS. In contrast, Zhuhai, Shenzhen, and Hong Kong, which are closest to the coast, have negative trends for both AMAX and NS.

The non-stationarity detected by the merged gridded dataset (Figures 1e–1g) is spatially consistent with the gauge-based results. For the 10-yr return period, the maximum trend (+12.2%/10 yr) (95% CI [11.7, 12.7]) for hourly rainfall is in central Guangzhou; comparable positive trends also occur in northwestern Huizhou (Figures 1f1 and 1f4). Negative trends in daily extremes around the southern coastlines (Zhuhai, Shenzhen, and Hong Kong) reach $-20\%/10$ yr. In addition, the southwest and east show a low degree of non-stationarity. If

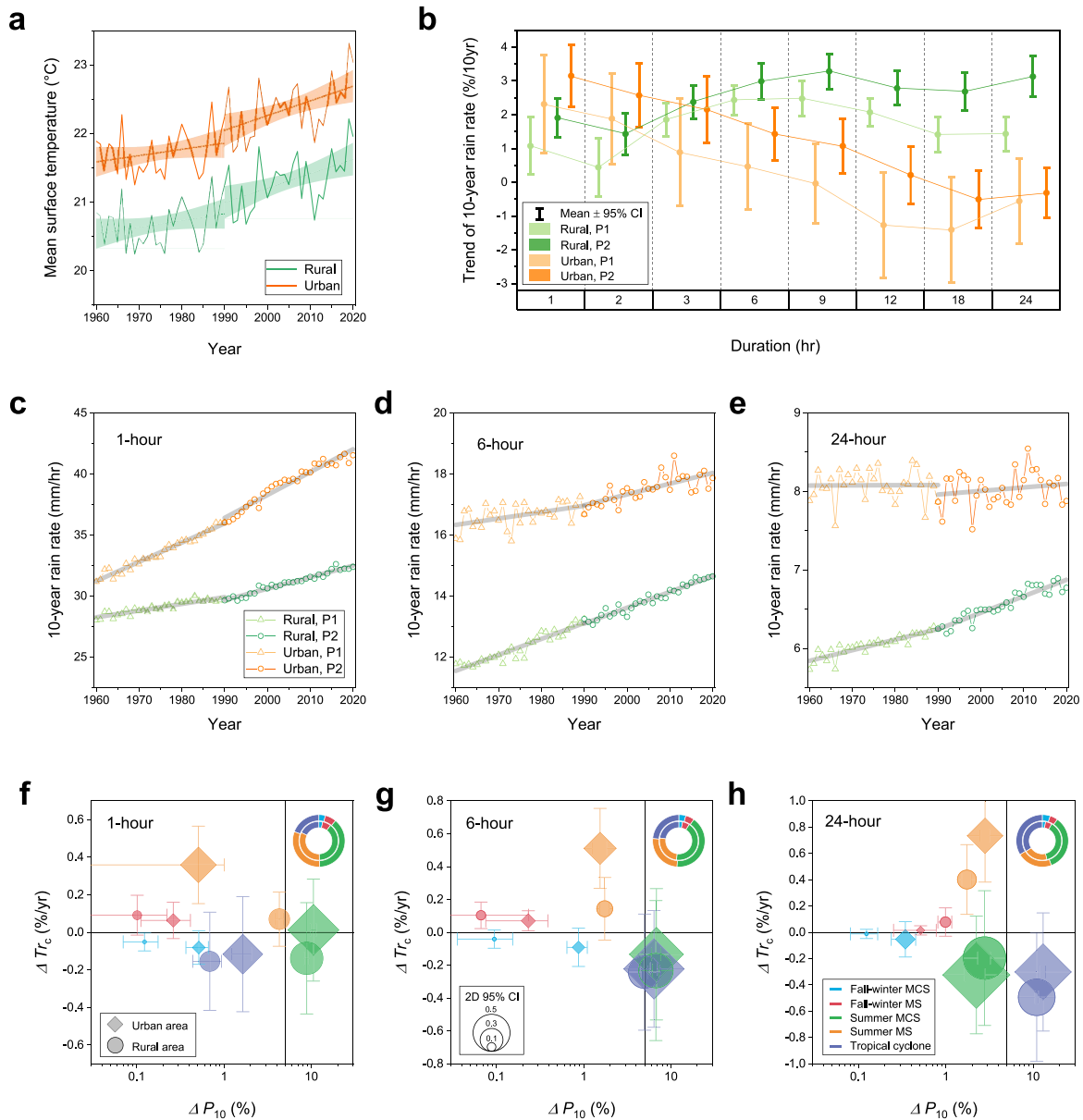


Figure 2. Non-stationarity in 10-yr rainfall extremes for urban and rural areas, and sensitivity to climate drivers. (a), median surface temperature time series and fitted linear trends for rural and urban areas for P1 (1960–1990) and P2 (1990–2020). (b) mean trends in extreme rainfall for rural and urban grid points and increasing event durations. (c)–(e), the median rainfall intensity and linear trends for rural and urban areas in Period 1 and Period 2 for 1-hr, 6-hr, and 24-hr durations, respectively. (g)–(h), Associations between 10-yr return period rainfall extremes and climate conditions at 1 hr, 6 and 24 hr durations. ΔP_{10} is the percent change in mean 10-yr return period intensity of the tested group; ΔTr_c is the annual trend in the intensity by group. Donut Charts in the top-right show the mean percentage contribution of each climate group, with inner and outer circles showing rural and urban areas, respectively.

stationary models are still applied, the errors (discrepancies from current-stage nonstationary results, calculated based on the covariates in 2020) spatially agree with the nonstationary patterns (Figure S3 in Supporting Information S1). Moreover, clusters with most rapidly increasing intensities tend to be located to the northeast of core urban regions (Figure S4 in Supporting Information S1), which may reflect the downwind effects of urban areas under prevailing southwesterlies and sea breezes (Han et al., 2014; Shepherd, 2013; Shepherd et al., 2010; Sun et al., 2021; Yang et al., 2021).

We also observe distinct spatial- and duration-dependent patterns in the non-stationarity (Figures 1e–1g). The largest area of significant non-stationarity occurred for the 1-hr duration at the 2-yr return period (Figure 2e1); over 1–24 hr durations, clusters of non-stationarity tend to shrink and retreat northwards; the proportion of the

study area with stationary rainfall extremes also expands. North-central and eastern Guangzhou plus northwestern Huizhou have increasing intensities for all return periods and durations, whereas negative-trend clusters extend inland from the southern coastlines especially for longer durations (12- to 24-hr). Accordingly, as the event duration increases, fewer grids are detected with nonstationary behavior (Figure S5 in Supporting Information S1) despite being penalized by the Akaike Information Criterion (AIC) due to an increased number of model parameters (Text S2 in Supporting Information S1). All cities except Zhaoqing and Jiangmen (in west GBA) are better represented by nonstationary than stationary models (Figure S6 in Supporting Information S1). According to the AIC, nonstationary models are favored at 98% of grids, across all durations (Figure S5 in Supporting Information S1).

3.2. Non-Stationarity With Land-Surface Dependency

The GBA has experienced rapid growth, with the urban land cover fraction increasing from 5% in 1980 to 15% in 2018 (Figure S4 in Supporting Information S1). Higher mean annual air temperatures (\bar{T}_y) are observed in 1990–2020 (P2) compared with 1960–1990 (P1) (Figure 2a). Grids classified as urban or rural have similar trends in \bar{T}_y (respectively +0.080°C/10 yr and +0.084°C/10 yr in P1, and +0.243°C/10 yr and +0.237°C/10 yr in P2). However, major differences in rainfall extremes emerge between the urban and rural groups at different event durations (Figure 2b). The urban group has stronger trends than the rural group for short durations (1–2 hr), whereas this pattern is reversed for longer durations (6–24 hr). The 3-hr duration appear to be the threshold for distinguishing rural-urban influences. Furthermore, trends in P2 are generally greater than those in P1, coincident with trends in mean surface air temperature.

Regional non-stationarity in the median of 10-yr intensities for all grids in the corresponding groups (Figures 2c–2e) agree with the mean statistics in Figure 2b. Interestingly, during P2, the 1 hr 10-yr rainfall intensity increased much faster in urban (+1.88 mm/hr/10 yr, 95% CI [1.79, 1.96]) than rural areas (+0.94 mm/hr/10 yr, 95% CI [0.90, 0.98]) (Figure 2c). However, the difference between urban and rural trends is less at 6 hr duration (Figure 2d), then the urban rate is overtaken by rural areas at 24 hr duration (+0.045 mm/hr/10 yr, 95% CI [0.001, 0.009], vs. +0.210 mm/hr/10 yr, 95% CI [0.195, 0.226], Figure 2e). These findings highlight the importance of differentiating between event durations when making distinctions in urban-rural rainfall extremes and associated changes in long-term flood risk at regional scales.

3.3. Potential Drivers of Non-Stationarity in Rainfall Extremes

Non-stationary rainfall extremes are likely associated with changing atmospheric conditions at local, regional and global scales (Slater et al., 2021). Heavy rainfall events mainly occur over southern China during the East Asia summer monsoon (MS) and tropical cyclone (TC) landfalls (Lai et al., 2020; Tang et al., 2021). In the Pearl River Basin where the GBA is located, mesoscale convective systems (MCS) contribute a significant portion of rainfall extremes during monsoons, particularly for the Pre-Meiyu and Meiyu period (mainly in May and June) when southwesterlies prevail (Chen et al., 2019; Cheng et al., 2022). We relate rainfall extremes (≥ 99 th percentiles) in each grid to one of five types of events, namely (a) TC; MCS during (b) summer and (c) fall-to-early winter MS periods; and other weather during the (d) summer and (e) fall-winter periods. Then, we perform the nonstationary frequency analysis with respect to each of the climate activities while excluding the associated AMAX (Text S4 in Supporting Information S1).

In terms of 10-yr rainfall intensities, we find that summer MCSs and TCs exhibit the highest sensitivity ($\Delta P_{10} \sim 10\%$) at 1 and 24 hr durations, respectively (Figures 2f–2h). And they are comparably important for the 6-hr duration, consistent with the typical lifetime of the associated weather systems (Li, Fowler, et al., 2020; Li, Moseley, et al., 2020; Liu & Wang, 2020). Summer MS also contribute non-negligibly over the three event durations (1%–5%). As for the occurrence frequencies in association with rainfall extremes, TCs account for a larger fraction over longer durations (rising from 18% to 34%, for 1–24 hr durations), but the annual trend (%) gradually decreases. Although the slowdown of TCs landfalling speeds and increasing stalling frequencies are expected to bring higher total precipitation to the Pearl River Delta (Hall & Kossin, 2019; Lai et al., 2020; Zhang et al., 2023), we observe a reduction in the duration of TC-induced rainfall extremes over the GBA (Figure S7 in Supporting Information S1). This is consistent with a decreased contribution of TCs (negative ΔTr_c) to the occurrence of rainfall extremes (≥ 99 th percentiles), in line with fewer TCs under global warming (Chand et al., 2022) particularly in low latitudes (Yamaguchi et al., 2020).

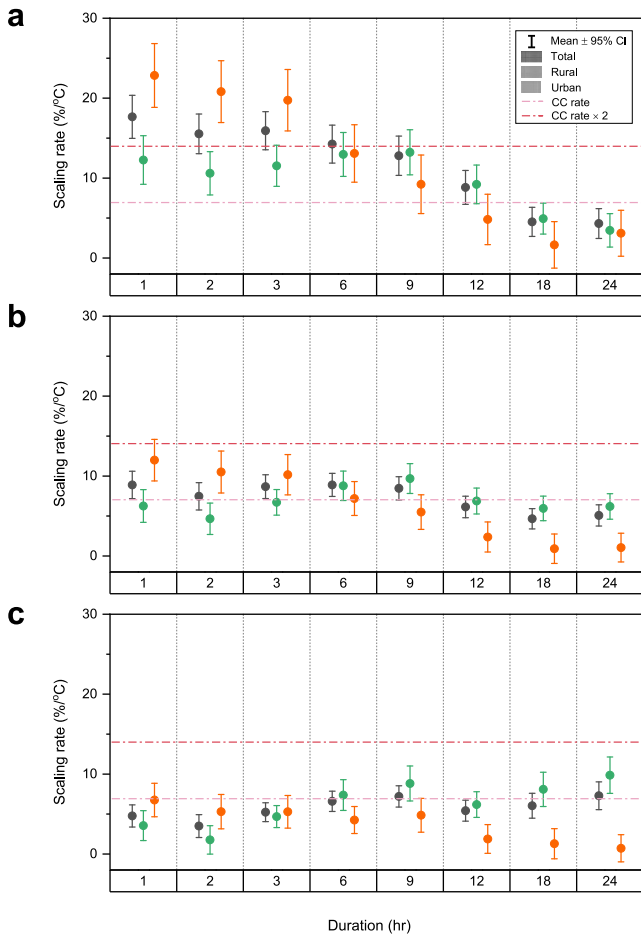


Figure 3. NS-RP scaling rates for (a) 2-, (b) 10- and (c) 100-yr return periods. Light and dark dashed lines denote C–C scaling (7%/°C) and super C–C rates (14%/°C, or C–C × 2), respectively.

A marked rise in contribution of summer MS to rainfall extremes is observed especially for urban areas. This suggests that smaller-scale convective systems (as well as monsoon patterns) are increasingly associate with the non-stationarity. In fact, meso- β - to meso- γ - scale storms (2–200 km) constitute a considerable portion of extreme rainfall events in the GBA (Sun et al., 2021), but are likely to be represented by the MS group due to resolution constraints of gridded infrared brightness temperature data (4–30 km) (Cheng et al., 2022; Huang et al., 2018). Furthermore, the change of contribution of MCSs to rainfall extremes is relatively modest, and the frequency of fall-to-early winter activities remains stable. Besides the 10-yr return period presented above, similar patterns are found for 2- (Figure S8 in Supporting Information S1) and 100-yr (Figure S9 in Supporting Information S1) return periods although the uncertainty represented by confidence intervals expands with return period.

3.4. Temperature Scaling of Non-Stationary Rainfall Extremes

Nonstationary rainfall intensities for various return periods are paired with the AMSAT to obtain the NS-RP scaling (Section 2.5). Overall, the total (rural + urban) scaling rates vary around the C–C ($\sim 7\%/^{\circ}\text{C}$) and super C–C rate (14%/°C), peaking for 1 hr (17.7%/°C), 6 hr (8.9%/°C) and 24 hr (7.3%/°C) durations for 2-, 10- and 100-yr RPs respectively, with marked rural-urban contrasts (Figure 3). Scaling for urban areas peaks at 1 hr duration (22.9%/°C), remains high to 3-hr duration (19.9%/°C), then declines for longer durations and return periods. Conversely, rural areas have peak scaling at, or longer than, 9-hr duration with less variation across all durations. Short-duration scaling rates tend to decline with increasing RPs, but not for longer durations (≥ 9 hr). The above patterns agree well with the scaling rates derived from regional median rainfall intensities (Figure S10 in Supporting Information S1). Moreover, 80% and 26% of the urban and rural areas respectively in the GBA are at elevations <60 m (Figure S6 in Supporting Information S1), such that elevation-related temperature differences between urban and rural areas may confound the effects of land cover. We thus recalculate scaling rates excluding grids with elevation >100 m (leaving 62%

of the GBA). The results show marginal differences in terms of scaling rates and rural-urban contrasts (Figure S11 in Supporting Information S1), underlining the dominant effect of land cover on sub-regional variations in NS-RP scaling.

It may not be plausible to claim the behavior of NS-RP scaling rates based on the C–C relation, as the AMSAT rather than event-associated temperature is adopted in the scaling, and the extremity is far beyond commonly inspected “heavy rainfall” (e.g., 90th to 99.9th percentile in each temperature bin). However, similar to the C–C relation, purely thermodynamic considerations yield a constant scaling rate ($\sim 7\%/^{\circ}\text{C}$) and cannot explain the remarkably large variations across durations and sensitivities to land cover, which signify strong controls from dynamic conditions (Berg et al., 2013; Lenderink et al., 2017). Although a higher temperature is generally favorable for convective precipitation (Fowler et al., 2021), negative gradients for the temperature-precipitation scaling are widely observed above certain temperature thresholds (Berg et al., 2013; Oh et al., 2021; Visser et al., 2021), owing to the lack of moisture availability as relative humidity decreases even for humid climates (Chan et al., 2016; Lenderink & Van Meijgaard, 2010; Sun & Wang, 2022). Higher surface temperatures (Figure 2a) render urban areas to be more susceptible to such humidity limitation at long durations compared to rural areas, and thus smaller scaling rates under the same amount of regional warming (Figure 3). In fact, a negative contribution of urbanization to daily-scale precipitation extremes – attributed to urban dry island effects – has been observed in many China coastal urban agglomerations including the GBA (Lin et al., 2020). Conversely, urban heat island effects are known to enhance short-lived rainfall extremes (Chang et al., 2023; Huang et al., 2022; Li, Fowler, et al., 2020; Li, Moseley, et al., 2020). In addition, downwind effects (Section 3.1) of urbanization, the distance of which depends on the organization degree of convection, further complicate

scaling patterns (Naylor & Mulholland, 2023). An improved understanding of the underlying dynamics requires differentiation of rainfall generating mechanisms and atmospheric dynamics at event scales.

4. Discussion and Conclusion

Our study demonstrates time- and space-scaling of non-stationarity in rainfall extremes over the rapidly developing GBA. We detect more severe rainfall extremes over the north-central region of the megalopolis compared with southern coastlines. We also reveal the contribution by urban areas to non-stationarity in short-duration (<6 hr) rainfall extremes in contrast to more uniform uplift across all event durations over rural areas. These findings are further supported variations in temperature-scaling observed for different return periods. Remarkably high scaling rates are detected for short duration events in urban areas, but these wane with increasing durations. This highlights the exacerbation of the rainfall extremes by urbanization at short time scales, on top of their overall intensification under a warming climate.

Opinions vary as to whether rainfall extremes have nonstationary frequencies, and whether to adopt nonstationary models to adjust local climate allowances for infrastructure design (Agilan & Umamahesh, 2016; Ganguli & Coulibaly, 2017; Sarhadi & Soulis, 2017; Vu & Mishra, 2019; Westra et al., 2014; Yilmaz et al., 2014). However, the heterogeneous duration- and land-cover dependent non-stationarity (e.g., Figures 2b and 3), which also exhibits spatial scale-dependent variabilities, suggests that more nuanced approaches to flood risk assessment and management are needed (Yan et al., 2023). At regional scales (~100 km), variations in non-stationarity are detected in the annual trends of return periods for urban and rural subgroups (Figure 2b) and integrated in the NS-RP scaling (Figure 3). At the grid scale (~10 km), significant spatial disparities exist (Figures 1e–1g), implying the need for distinct strategies to update IDF curves. For example, a clockwise rotation of IDF curves is expected in Shenzhen and Hong Kong, as opposed to Dongguan, while those for Guangdong may see an overall uplift. Additionally, point-scale non-stationarity (Figures 1b and 1d) may further deviate from the grid-scale (Figures 1e and 1g). Hence, we recommend description of upper-tail statistics distinguishing spatiotemporal scales and land cover type of interest.

This study is among the first to apply a multi-source merged and high spatiotemporal-resolution rainfall dataset to nonstationary frequency analysis. This avoids the drawbacks of sparse, localized, and uneven rain gauge networks (Kidd et al., 2017; Lengfeld et al., 2020), relatively poor accuracy of satellite and reanalysis products (Alexander et al., 2019; Ali et al., 2021), and high computational costs and input uncertainties associated with numerical weather model experiments (Alexander et al., 2019; Sun et al., 2021). However, finer-scale extreme events due to deep convection systems (~1 km) (Lengfeld et al., 2020; Shepherd et al., 2002), highly localized (or slow-moving) short-duration storms around urban agglomerations (Sun et al., 2021), may still be omitted by our blended dataset. Radar data are needed to capture sub-hourly rainfall extremes at 1 km resolution (Ayat et al., 2022; Lengfeld et al., 2020), but were not applied here due to their short records (<20 yr). This challenge is not unique to the Greater Bay Area and is a global challenge (Lengfeld et al., 2020). Future efforts to investigate highly localized changes in rainfall extremes would be assisted by denser rain gauge networks, more radar reflectivity measurements and numerical simulations.

In summary, we provide systematic evidence of the intensification of rainfall extremes over the areas with higher degree of urbanization in a coastal megalopolis. This amplification is nonlinearly biased toward short (~2-yr) return periods and short durations (<6 hr), especially in urban areas. The tendency for more frequent “nuisance” events may have less dramatic consequences but nonetheless pose recurrent challenges for urban transport and drainage infrastructure (Fowler et al., 2021). This will require adaptations to increasing risk of flash floods and protection measures for vulnerable people (Yin et al., 2023). Such detail is often missed at continental- and event-scales due to coarse resolution data and short rainfall records. However, a more sophisticated approach to rainfall extremes is needed to bridge the gap between atmospheric science and flood hydrology (Westra et al., 2014). Our results show that the assumption that sub-daily rainfall extremes scale with global warming at the same rate over urban and rural surfaces is no longer tenable. This has major implications for climate change allowances used by engineers when designing infrastructure in rapidly growing tropical cities. Further research is needed to test whether the same land cover dependencies are observed in other climate regimes.

Conflict of Interest

The authors declare no conflicts of interest relevant to this study.

Data Availability Statement

The hourly precipitation data of rain gauges can be obtained from China Meteorological Administration (2023) for Guangdong stations and Hong Kong Observatory (2023) for Hong Kong stations. The MSWEP V.2.8 gridded precipitation data are available at Beck et al. (2019). The IMERG V07 data are available at Huffman et al. (2023). The Era5-Land reanalysis data including hourly gridded precipitation, surface (2m above ground) temperature and dew point temperature were obtained from Copernicus Climate Change Service (2022). The global annual land–ocean temperature time series were obtained from NOAA Merged Land Ocean Global Surface Temperature Analysis (Huang et al., 2023). The Multivariate ENSO Index time series (Version 2) were obtained from The NOAA Physical Sciences Laboratory (PSL) (2023). The FABDEM terrain data was sourced from Hawker and Neal (2021). Land cover data covering the Greater Bay Area were obtained from Xu et al. (2018). The MCS datasets can be accessed from Huang et al. (2018) and Cheng et al. (2022). The International Best Track Archive for Climate Stewardship (IBTrACS) can be obtained at Knapp et al. (2010, 2018). The merged and corrected gridded hourly precipitation dataset over the GBA, as well as scripts for data processing and analysis, can be accessed in the Zenodo repository (Yan & Guan, 2024).

Acknowledgments

This work is financially supported by General Research Fund projects (No. 17202020, No. 17210923) from Hong Kong Research Grants Council, Environment and Conservation Fund Project (ref: 108/2019) from Hong Kong Environmental Protection Department, and the National Natural Science Foundation of China (Grant 42371076). X.C. received funding from National Key Research and Development Program of China for Intergovernmental Cooperation (2019YFE01110100), Science and technology innovation team project of Guangdong Meteorological Bureau (GRMCTD202104) and the National Natural Science Foundation of China (41975124).

References

- Agilan, V., & Umamahesh, N. V. (2015). Detection and attribution of non-stationarity in intensity and frequency of daily and 4-h extreme rainfall of Hyderabad, India. *Journal of Hydrology*, 530, 677–697. <https://doi.org/10.1016/j.jhydrol.2015.10.028>
- Agilan, V., & Umamahesh, N. V. (2016). Is the covariate based non-stationary rainfall IDF curve capable of encompassing future rainfall changes? *Journal of Hydrology*, 541, 1441–1455. <https://doi.org/10.1016/j.jhydrol.2016.08.052>
- Alexander, L. V., Fowler, H. J., Bador, M., Behrangi, A., Donat, M. G., Dunn, R., et al. (2019). On the use of indices to study extreme precipitation on sub-daily and daily timescales. *Environmental Research Letters*, 14(12), 125008. <https://doi.org/10.1088/1748-9326/ab51b6>
- Ali, H., Fowler, H. J., Lenderink, G., Lewis, E., & Pritchard, D. (2021). Consistent large-scale response of hourly extreme precipitation to temperature variation over land. *Geophysical Research Letters*, 48(4). <https://doi.org/10.1029/2020GL090317>
- Ayat, H., Evans, J. P., Sherwood, S. C., & Soderholm, J. (2022). Intensification of subhourly heavy rainfall. *Science*, 378(6620), 655–659. <https://doi.org/10.1126/science.abn8657>
- Baez-Villanueva, O. M., Zambrano-Bigiarini, M., Beck, H. E., McNamara, I., Ribbe, L., Nauditt, A., et al. (2020). RF-MEP: A novel Random Forest method for merging gridded precipitation products and ground-based measurements. *Remote Sensing of Environment*, 239, 111606. <https://doi.org/10.1016/j.rse.2019.111606>
- Bao, J., Sherwood, S. C., Alexander, L. V., & Evans, J. P. (2017). Future increases in extreme precipitation exceed observed scaling rates. *Nature Climate Change*, 7(2), 128–132. <https://doi.org/10.1038/nclimate3201>
- Barbero, R., Fowler, H. J., Lenderink, G., & Blenkinsop, S. (2017). Is the intensification of precipitation extremes with global warming better detected at hourly than daily resolutions? *Geophysical Research Letters*. <https://doi.org/10.1002/2016GL071917>
- Beck, H. E., Wood, E. F., Pan, M., Fisher, C. K., Miralles, D. G., van Dijk, A. I. J. M., et al. (2019). MSWEP V2 global 3-hourly 0.1° precipitation: Methodology and quantitative assessment. *Bulletin of the American Meteorological Society*, 100(3), 473–500. <https://doi.org/10.1175/BAMS-D-17-0138.1>
- Berg, P., Moseley, C., & Haerter, J. O. (2013). Strong increase in convective precipitation in response to higher temperatures. *Nature Geoscience*, 6(3), 181–185. <https://doi.org/10.1038/ngeo1731>
- Chan, S. C., Kendon, E. J., Roberts, N. M., Fowler, H. J., & Blenkinsop, S. (2016). Downturn in scaling of UK extreme rainfall with temperature for future hottest days. *Nature Geoscience*, 9(1), 24–28. <https://doi.org/10.1038/ngeo2596>
- Chand, S. S., Walsh, K. J. E., Camargo, S. J., Kossin, J. P., Tory, K. J., Wehner, M. F., et al. (2022). Declining tropical cyclone frequency under global warming. *Nature Climate Change*, 12(7), 655–661. <https://doi.org/10.1038/s41558-022-01388-4>
- Chang, C., Chen, Y., & Huang, J. J. (2023). A comparison study on the role of urbanization in altering the short-duration and long-duration intense rainfall. *The Science of the Total Environment*, 857, 159290. <https://doi.org/10.1016/j.scitotenv.2022.159290>
- Chen, D., Guo, J., Yao, D., Lin, Y., Zhao, C., Min, M., et al. (2019). Mesoscale convective systems in the Asian monsoon region from advanced Himawari Imager: Algorithms and preliminary results. *Journal of Geophysical Research: Atmospheres*, 124(4), 2210–2234. <https://doi.org/10.1029/2018JD029707>
- Chen, Y., Liao, Z., Shi, Y., Tian, Y., & Zhai, P. (2021). Detectable increases in sequential flood-heatwave events across China during 1961–2018. *Geophysical Research Letters*, 48(6). <https://doi.org/10.1029/2021GL092549>
- Chen, Y.-R., Yu, B., & Jenkins, G. (2013). Secular variation in rainfall and intensity–frequency–duration curves in Eastern Australia. *Journal of Water and Climate Change*, 4(3), 244–251. <https://doi.org/10.2166/wcc.2013.138>
- Cheng, T. F., Dong, Q., Dai, L., & Lu, M. (2022). A dual regime of mesoscale convective systems in the East Asian monsoon annual cycle. *Journal of Geophysical Research: Atmospheres*, 127(13). <https://doi.org/10.1029/2022JD036523>
- China Meteorological Administration. (2023). Daily timed data from automated weather stations in China [Dataset]. China Meteorological Administration National Meteorological Information Center. Retrieved from <https://data.cma.cn/en/?r=data/detail&dataCode=A.0012.0001>
- Coles, S., Pericchi, L. R., & Sisson, S. (2003). A fully probabilistic approach to extreme rainfall modeling. *Journal of Hydrology*, 273(1–4), 35–50. [https://doi.org/10.1016/S0022-1694\(02\)00353-0](https://doi.org/10.1016/S0022-1694(02)00353-0)
- Copernicus Climate Change Service. (2022). ERA5-Land hourly data from 1950 to present. [Dataset]. Copernicus Climate Change Service (C3S) Climate Data Store (CDS). <https://doi.org/10.24381/cds.e2161bac>
- Fauer, F. S., & Rust, H. W. (2022). Non-stationary large-scale statistics of precipitation extremes in central Europe. (arXiv:2211.04140). arXiv. Retrieved from <http://arxiv.org/abs/2211.04140>
- Fischer, E. M., & Knutti, R. (2016). Observed heavy precipitation increase confirms theory and early models. *Nature Climate Change*, 6(11), 986–991. <https://doi.org/10.1038/nclimate3110>
- Fowler, H. J., Lenderink, G., Prein, A. F., Westra, S., Allan, R. P., Ban, N., et al. (2021). Anthropogenic intensification of short-duration rainfall extremes. *Nature Reviews Earth and Environment*, 2(2), 107–122. <https://doi.org/10.1038/s43017-020-00128-6>

- Fu, G., Chiew, F. H., Zheng, H., Robertson, D. E., Potter, N. J., Teng, J., et al. (2021). Statistical analysis of attributions of climatic characteristics to nonstationary rainfall-streamflow relationship. *Journal of Hydrology*, *603*, 127017. <https://doi.org/10.1016/j.jhydrol.2021.127017>
- Ganguli, P., & Coulibaly, P. (2017). Does nonstationarity in rainfall require nonstationary intensity–duration–frequency curves? *Hydrology and Earth System Sciences*, *21*(12), 6461–6483. <https://doi.org/10.5194/hess-21-6461-2017>
- Gocic, M., & Trajkovic, S. (2013). Analysis of changes in meteorological variables using Mann-Kendall and Sen's slope estimator statistical tests in Serbia. *Global and Planetary Change*, *100*, 172–182. <https://doi.org/10.1016/j.gloplacha.2012.10.014>
- Grimm, N. B., Faeth, S. H., Golubiewski, N. E., Redman, C. L., Wu, J., Bai, X., & Briggs, J. M. (2008). Global change and the ecology of cities. *Science*, *319*(5864), 756–760. <https://doi.org/10.1126/science.1150195>
- Hall, T. M., & Kossin, J. P. (2019). Hurricane stalling along the North American coast and implications for rainfall. *Npj Climate and Atmospheric Science*, *2*(1), 17. <https://doi.org/10.1038/s41612-019-0074-8>
- Han, J.-Y., Baik, J.-J., & Lee, H. (2014). Urban impacts on precipitation. *Asia-Pacific Journal of Atmospheric Sciences*, *50*(1), 17–30. <https://doi.org/10.1007/s13143-014-0016-7>
- Hawker, L., & Neal, J. (2021). FABDEM V1-0. [Dataset]. <https://doi.org/10.5523/bris.25wfy0f9ukoge2gs7a5mqpq2j7>
- Hersbach, H., Bell, B., Berrisford, P., Hirahara, S., Horányi, A., Muñoz-Sabater, J., et al. (2020). The ERA5 global reanalysis. *Quarterly Journal of the Royal Meteorological Society*, *146*(730), 1999–2049. <https://doi.org/10.1002/qj.3803>
- Hong Kong Observatory. (2023). Hourly precipitation observations from individual weather stations. [Dataset]. Hong Kong Observatory Climatological Information Services. Retrieved from <https://www.hko.gov.hk/en/cis/climat.htm>
- Hosseinzadehtalaei, P., Tabari, H., & Willems, P. (2020). Climate change impact on short-duration extreme precipitation and intensity–duration–frequency curves over Europe. *Journal of Hydrology*, *590*, 125249. <https://doi.org/10.1016/j.jhydrol.2020.125249>
- Huang, B., Yin, X., Menne, M. J., Vose, R., & Zhang, H. (2023). NOAA Global Surface Temperature Dataset (NOAAGlobalTemp), Version 6.0.0. [Dataset]. NOAA National Centers for Environmental Information. <https://www.ncei.noaa.gov/metadata/geoportal/rest/metadata/item/gov.noaa.ncdc%3AC01704/html>
- Huang, J., Fatichi, S., Mascaro, G., Manoli, G., & Peleg, N. (2022). Intensification of sub-daily rainfall extremes in a low-rise urban area. *Urban Climate*, *42*, 101124. <https://doi.org/10.1016/j.uclim.2022.101124>
- Huang, X., Hu, C., Huang, X., Chu, Y., Tseng, Y., Zhang, G. J., & Lin, Y. (2018). A long-term tropical mesoscale convective systems dataset based on a novel objective automatic tracking algorithm. *Climate Dynamics*, *51*(7–8), 3145–3159. <https://doi.org/10.1007/s00382-018-4071-0>
- Huffman, G. J., Bolvin, D. T., Joyce, R., Nelkin, E. J., Tan, J., Hsu, K., et al. (2023). NASA Global Precipitation Measurement (GPM) Integrated Multi-satellite Retrievals for GPM (IMERG) Version 07. [Dataset]. https://disc.gsfc.nasa.gov/datasets/GPM_3IMERGHH_07/summary?keywords=%22IMERG%20final%22
- IPCC. (2021). *Climate change 2021: The physical science basis. Contribution of working group I to the sixth assessment report of the intergovernmental panel on climate change*. In Masson-Delmotte, V. P. Zhai, A. Pirani, S. L. Connors, C. Péan, et al. (Eds.).
- Khalik, M. N., Ouarda, T. B. M. J., Gachon, P., Sushama, L., & St-Hilaire, A. (2009). Identification of hydrological trends in the presence of serial and cross correlations: A review of selected methods and their application to annual flow regimes of Canadian rivers. *Journal of Hydrology*, *368*(1–4), 117–130. <https://doi.org/10.1016/j.jhydrol.2009.01.035>
- Khalik, M. N., Ouarda, T. B. M. J., Ondo, J.-C., Gachon, P., & Bobée, B. (2006). Frequency analysis of a sequence of dependent and/or nonstationary hydro-meteorological observations: A review. *Journal of Hydrology*, *329*(3–4), 534–552. <https://doi.org/10.1016/j.jhydrol.2006.03.004>
- Kidd, C., Becker, A., Huffman, G. J., Muller, C. L., Joe, P., Skofronick-Jackson, G., & Kirschbaum, D. B. (2017). So, how much of the Earth's surface is covered by rain gauges? *Bulletin of the American Meteorological Society*, *98*(1), 69–78. <https://doi.org/10.1175/BAMS-D-14-00283.1>
- Knapp, K. R., Diamond, H. J., Kossin, J. P., Kruk, M. C., & Schreck, C. J. (2018). International Best Track Archive for Climate Stewardship (IBTrACS) Project, Version 4. [Dataset]. NOAA National Centers for Environmental Information. <https://doi.org/10.25921/82ty-9e16>
- Knapp, K. R., Kruk, M. C., Levinson, D. H., Diamond, H. J., & Neumann, C. J. (2010). The International Best Track Archive for Climate Stewardship (IBTrACS): Unifying tropical cyclone best track data. *Bulletin of the American Meteorological Society*, *91*(3), 363–376. <https://doi.org/10.1175/2009BAMS2755.1>
- Lai, Y., Li, J., Gu, X., Chen, Y. D., Kong, D., Gan, T. Y., et al. (2020). Greater flood risks in response to slowdown of tropical cyclones over the coast of China. *Proceedings of the National Academy of Sciences*, *117*(26), 14751–14755. <https://doi.org/10.1073/pnas.1918987117>
- Lenderink, G., Barbero, R., Loriaux, J. M., & Fowler, H. J. (2017). Super-clausius–clapeyron scaling of extreme hourly convective precipitation and its relation to large-scale atmospheric conditions. *Journal of Climate*, *30*(15), 6037–6052. <https://doi.org/10.1175/JCLI-D-16-0808.1>
- Lenderink, G., & van Meijgaard, E. (2008). Increase in hourly precipitation extremes beyond expectations from temperature changes. *Nature Geoscience*, *1*(8), 511–514. <https://doi.org/10.1038/ngeo262>
- Lenderink, G., & Van Meijgaard, E. (2010). Linking increases in hourly precipitation extremes to atmospheric temperature and moisture changes. *Environmental Research Letters*, *5*(2), 025208. <https://doi.org/10.1088/1748-9326/5/2/025208>
- Lengfeld, K., Kirstetter, P.-E., Fowler, H. J., Yu, J., Becker, A., Flamig, Z., & Gourley, J. (2020). Use of radar data for characterizing extreme precipitation at fine scales and short durations. *Environmental Research Letters*, *15*(8), 085003. <https://doi.org/10.1088/1748-9326/ab98b4>
- Li, P., Moseley, C., Prein, A. F., Chen, H., Li, J., Furtado, K., & Zhou, T. (2020). Mesoscale convective system precipitation characteristics over East Asia. Part I: Regional differences and seasonal variations. *Journal of Climate*, *33*(21), 9271–9286. <https://doi.org/10.1175/JCLI-D-20-0072.1>
- Li, Y., Fowler, H. J., Argüeso, D., Blenkinsop, S., Evans, J. P., Lenderink, G., et al. (2020). Strong intensification of hourly rainfall extremes by urbanization. *Geophysical Research Letters*, *47*(14). <https://doi.org/10.1029/2020GL088758>
- Lin, L., Gao, T., Luo, M., Ge, E., Yang, Y., Liu, Z., et al. (2020). Contribution of urbanization to the changes in extreme climate events in urban agglomerations across China. *The Science of the Total Environment*, *744*, 140264. <https://doi.org/10.1016/j.scitotenv.2020.140264>
- Liu, J., & Niyogi, D. (2019). Meta-analysis of urbanization impact on rainfall modification. *Scientific Reports*, *9*(1), 7301. <https://doi.org/10.1038/s41598-019-42494-2>
- Liu, L., & Wang, Y. (2020). Trends in landfalling tropical cyclone-induced precipitation over China. *Journal of Climate*, *33*(6), 2223–2235. <https://doi.org/10.1175/JCLI-D-19-0693.1>
- McLeod, J., & Shepherd, M. (2022). A synoptic framework for forecasting the urban rainfall effect using composite and K-means cluster analyses. *Frontiers in Environmental Science*, *10*, 808026. <https://doi.org/10.3389/fenvs.2022.808026>
- McLeod, J., Shepherd, M., & Konrad, C. E. (2017). Spatio-temporal rainfall patterns around Atlanta, Georgia and possible relationships to urban land cover. *Urban Climate*, *21*, 27–42. <https://doi.org/10.1016/j.uclim.2017.03.004>
- Milly, P. C. D., Betancourt, J., Falkenmark, M., Hirsch, R. M., Kundzewicz, Z. W., Lettenmaier, D. P., & Stouffer, R. J. (2008). Stationarity is dead: Whither water management? (p. 319). <https://doi.org/10.1126/science.1151915>

- Naylor, J., & Mulholland, J. P. (2023). The impact of vertical wind shear on the outcome of interactions between squall lines and cities. *Journal of Geophysical Research: Atmospheres*, 128(3), e2022JD037237. <https://doi.org/10.1029/2022JD037237>
- Nerantzaki, S. D., & Papalexiou, S. M. (2022). Assessing extremes in hydroclimatology: A review on probabilistic methods. *Journal of Hydrology*, 605, 127302. <https://doi.org/10.1016/j.jhydrol.2021.127302>
- NOAA Physical Sciences Laboratory (PSL). (2023). Multivariate ENSO Index Version 2 (MEI.v2). [Dataset]. The NOAA Physical Sciences Laboratory (PSL). Retrieved from <https://psl.noaa.gov/enso/mei/>
- Oh, S.-G., Son, S.-W., & Min, S.-K. (2021). Possible impact of urbanization on extreme precipitation–temperature relationship in East Asian megacities. *Weather and Climate Extremes*, 34, 100401. <https://doi.org/10.1016/j.wace.2021.100401>
- Papalexiou, S. M., & Montanari, A. (2019). Global and regional increase of precipitation extremes under global warming. *Water Resources Research*, 55(6), 4901–4914. <https://doi.org/10.1029/2018WR024067>
- Qiang, Y., Zhang, L., & Xiao, T. (2020). Spatial-temporal rain field generation for the Guangdong-Hong Kong-Macau Greater Bay Area considering climate change. *Journal of Hydrology*, 583, 124584. <https://doi.org/10.1016/j.jhydrol.2020.124584>
- Sarhadi, A., & Soulis, E. D. (2017). Time-varying extreme rainfall intensity-duration-frequency curves in a changing climate. *Geophysical Research Letters*, 44(5), 2454–2463. <https://doi.org/10.1002/2016GL072201>
- Schelske, O., Sundermann, L., & Hausmann, P. (2013). Mind the risk—A global ranking of cities under threat from natural disasters. *Swiss Re*. Shepherd, J. M. (2013). *Impacts of urbanization on precipitation and storms: Physical insights and vulnerabilities*. In *Climate Vulnerability* (pp. 109–125). Elsevier. <https://doi.org/10.1016/B978-0-12-384703-4.00503-7>
- Shepherd, J. M., Carter, M., Manyin, M., Messen, D., & Burian, S. (2010). The impact of urbanization on current and future coastal precipitation: A case study for Houston. *Environment and Planning B: Planning and Design*, 37(2), 284–304. <https://doi.org/10.1068/b34102t>
- Shepherd, J. M., Pierce, H., & Negri, A. J. (2002). Rainfall modification by major urban areas: Observations from spaceborne rain radar on the TRMM satellite. *Journal of Applied Meteorology*, 41(7), 689–701. [https://doi.org/10.1175/1520-0450\(2002\)041<0689:RMBMUA>2.0.CO;2](https://doi.org/10.1175/1520-0450(2002)041<0689:RMBMUA>2.0.CO;2)
- Slater, L. J., Anderson, B., Buechel, M., Dadson, S., Han, S., Harrigan, S., et al. (2021). Nonstationary weather and water extremes: A review of methods for their detection, attribution, and management. *Hydrology and Earth System Sciences*, 25(7), 3897–3935. <https://doi.org/10.5194/hess-25-3897-2021>
- Song, F., Zhang, G. J., Ramanathan, V., & Leung, L. R. (2022). Trends in surface equivalent potential temperature: A more comprehensive metric for global warming and weather extremes. *Proceedings of the National Academy of Sciences*, 119(6), e2117832119. <https://doi.org/10.1073/pnas.2117832119>
- Sun, Q., Miao, C., Duan, Q., Ashouri, H., Sorooshian, S., & Hsu, K. (2018). A review of global precipitation data sets: Data sources, estimation, and intercomparisons. *Reviews of Geophysics*, 56(1), 79–107. <https://doi.org/10.1002/2017RG000574>
- Sun, X., Luo, Y., Gao, X., Wu, M., Li, M., Huang, L., et al. (2021). On the localized extreme rainfall over the Great Bay area in south China with complex topography and strong UHI effects. *Monthly Weather Review*, 149(8), 2777–2801. <https://doi.org/10.1175/MWR-D-21-0004.1>
- Sun, X., & Wang, G. (2022). Causes for the negative scaling of extreme precipitation at high temperatures. *Journal of Climate*, 35(18), 6119–6134. <https://doi.org/10.1175/JCLI-D-22-0142.1>
- Tang, Y., Huang, A., Wu, P., Huang, D., Xue, D., & Wu, Y. (2021). Drivers of summer extreme precipitation events over East China. *Geophysical Research Letters*, 48(11). <https://doi.org/10.1029/2021GL093670>
- Visser, J. B., Wasko, C., Sharma, A., & Nathan, R. (2021). Eliminating the “hook” in precipitation–temperature scaling. *Journal of Climate*, 1–42. <https://doi.org/10.1175/JCLI-D-21-0292.1>
- Vu, T. M., & Mishra, A. K. (2019). Nonstationary frequency analysis of the recent extreme precipitation events in the United States. *Journal of Hydrology*, 575, 999–1010. <https://doi.org/10.1016/j.jhydrol.2019.05.090>
- Westra, S., Alexander, L. V., & Zwiers, F. W. (2013). Global increasing trends in annual maximum daily precipitation. *Journal of Climate*, 26(11), 3904–3918. <https://doi.org/10.1175/JCLI-D-12-00502.1>
- Westra, S., Fowler, H. J., Evans, J. P., Alexander, L. V., Berg, P., Johnson, F., et al. (2014). Future changes to the intensity and frequency of short-duration extreme rainfall: Future intensity of sub-daily rainfall. *Reviews of Geophysics*, 52(3), 522–555. <https://doi.org/10.1002/2014RG000464>
- Westra, S., & Sisson, S. A. (2011). Detection of non-stationarity in precipitation extremes using a max-stable process model. *Journal of Hydrology*, 406(1–2), 119–128. <https://doi.org/10.1016/j.jhydrol.2011.06.014>
- Xu, X., Liu, J., Zhang, S., Li, R., Yan, C., & Wu, S. (2018). China's multi-period land-use land-cover condition remote sensing monitoring data set (CNLUCC). [Dataset]. Institute of Geographic Sciences and Natural Resources Research of Chinese Academy of Sciences. <https://doi.org/10.12078/2018070201>
- Yamaguchi, M., Chan, J. C. L., Moon, I.-J., Yoshida, K., & Mizuta, R. (2020). Global warming changes tropical cyclone translation speed. *Nature Communications*, 11(1), 47. <https://doi.org/10.1038/s41467-019-13902-y>
- Yan, H., & Guan, M. (2024). Key data and code for "Urbanization further intensifies short-duration rainfall extremes in a warmer climate." [Dataset]. Zenodo. <https://doi.org/10.5281/zenodo.10715173>
- Yan, H., Guan, M., & Kong, Y. (2023). Flood retention lakes in a rural-urban catchment: Climate-dominated and configuration-affected performances. *Water Resources Research*, 59(8), e2022WR032911. <https://doi.org/10.1029/2022WR032911>
- Yang, L., Ni, G., Tian, F., & Niyogi, D. (2021). Urbanization exacerbated rainfall over European suburbs under a warming climate. *Geophysical Research Letters*, 48(21). <https://doi.org/10.1029/2021GL095987>
- Yilmaz, A. G., Hossain, I., & Perera, B. J. C. (2014). Effect of climate change and variability on extreme rainfall intensity–frequency–duration relationships: A case study of Melbourne. *Hydrology and Earth System Sciences*, 18(10), 4065–4076. <https://doi.org/10.5194/hess-18-4065-2014>
- Yin, J., Gao, Y., Chen, R., Yu, D., Wilby, R., Wright, N., et al. (2023). Flash floods: Why are more of them devastating the world's driest regions? *Nature*, 615(7951), 212–215. <https://doi.org/10.1038/d41586-023-00626-9>
- Zhang, J., Xu, J., Dai, X., Ruan, H., Liu, X., & Jing, W. (2022). Multi-source precipitation data merging for heavy rainfall events based on cokriging and machine learning methods. *Remote Sensing*, 14(7), 1750. <https://doi.org/10.3390/rs14071750>
- Zhang, L., Cheng, T. F., Lu, M., Xiong, R., & Gan, J. (2023). Tropical cyclone stalling shifts northward and brings increasing flood risks to east Asian coast. *Geophysical Research Letters*, 50(10), e2022GL102509. <https://doi.org/10.1029/2022GL102509>